

TABLE 6 Effect of Variation of Probe Feed Position

Probe Feed Position, p_{pos} (mm)	Resonant Frequency, f_r (GHz)	Return Loss, RL (dB)	Probe Feed Position, p_{pos} (mm)	Resonant Frequency, f_r (GHz)	Return Loss, R_L (dB)
0	8.98	-33.7	16	3.52	-13.1
1	3.53	-20.2	17	8.98	-29.8
2	4.62	-21.8	18	10.1	-14.4
3	2.41	-37.1	19	4.63	-17.8
4	2.44	-19.4	20	4.61	-13.6
5	7.89	-21.5	21	3.50	-25.3
6	8.28	-18.8	22	5.71	-31.63
7	12.2	-23.9	23	6.83	-12.3
8	5.73	-20.4	24	4.58	-32.7
9	4.61	-15.3	25	7.87	-35.7
10	5.21	-17.0	26	5.65	-30.0
11	7.28	-14.1	27	2.34	-25.6
12	6.74	-22.3	28	7.78	-25.5
13	6.37	-12.4	29	8.78	-37.1
14	3.54	-13.4	30	9.73	-35.8
15	3.53	-22.9	31	9.58	-23.2

$\epsilon_r = 4.78$, $h = 1.5$ mm, $w = 4.5$ mm, $l_1 = 33.8$ mm, $l_2 = 65.8$ mm, $\psi = 16^\circ$.

TABLE 7 Effect of Variation of Substrate Thickness on Bandwidth

Substrate Thickness, h (mm)	Inner Length of Arms, l_1 (mm)	Outer Length of Arms, l_2 (mm)	Probe Feed Position, p_{pos} (mm)	Bandwidth (MHz)
3.0	33.7	65.7	7.7	81
3.5	33.6	65.6	7.6	100
4.0	33.5	65.5	7.6	110
4.5	33.5	65.5	7.2	130
5.0	33.4	65.4	7.1	145
5.5	33.3	65.3	6.8	158
6.0	33.2	65.2	6.6	174

$\epsilon_r = 4.78$, $w = 4.5$ mm, $\psi = 16^\circ$, $f_r = 2.4$ GHz.

mm to 6.0 mm, the impedance bandwidth increases from 81 MHz to 174 MHz. So, by increasing the substrate thickness, the bandwidth can be enhanced. But, the substrate thickness cannot be increased to very much extent as the surface waves become dominant. Therefore, the substrate thickness has to be judiciously selected to get more bandwidth.

The simulated results are given for the V-shaped microstrip patch antenna with the following parameters: $\epsilon_r = 4.78$, $h = 4$ mm, $w = 4.5$ mm, $l_1 = 33.5$ mm, $l_2 = 65.5$ mm, and $\psi = 16^\circ$. Figure 11 shows the simulated return loss plot of the antenna. The resonant frequency of the patch is 2.4 GHz and the value of return loss at this frequency is -36.5 dB. The 10 dB return loss impedance bandwidth is found to be 110 MHz (4.6%).

4. CONCLUSION

A V-shaped microstrip patch antenna with coaxial probe feed has been designed. Its characteristics such as return loss, VSWR, impedance bandwidth, and far field radiation pattern are obtained by simulation using Ansoft HFSS software. The antenna has fairly small dimensions. The antenna performance depends upon the parameters ψ , p_{pos} , and w .

REFERENCES

1. C.A. Balanis, *Antenna Theory: Analysis and Design*, 2nd ed., Wiley, Hoboken, NJ 2008.
2. I.J. Bahl and P. Bhartia, *Microstrip Antennas*, Artech House Inc., Norwood, MA 1980.

3. C.L. Tang, J.Y. Chou, and K.L. Wong. Broadband dual-frequency v-shape patch antenna. *Microwave Opt Technol Lett* 25 (2000), 121–123.
4. D.M. Pozar and D.H. Schaubert, *Microstrip Antennas*, IEEE Press, New York, 1995.
5. S.H. Wi, Y.B. Sun, I.S. Song, S.H. Choa, I.S. Koh, Y.S. Lee, and J.G. Yook, Package-Level integrated antennas based on LTCC technology, *IEEE Trans Antennas Propag* 54 (2006), 2190–2197.
6. S.H. Wi, J.M. Kim, T.H. Yoo, H.J. Lee, J.Y. Park, J.G. Yook, and H.K. Park, Bow-tie shaped meander slot antenna for 5 GHz application, *Proc IEEE Int Symp Antenna Propag* 2 (2002), 456–459.
7. F. Yang, X. Zhang, and Y. Rahmat-Samii, Wide-band E-shaped patch antennas for wireless communications, *IEEE Trans Antennas Propag* 49 (2001), 1094–1100.

© 2011 Wiley Periodicals, Inc.

MICROSTRIP LOW PASS FILTER WITH WIDEBAND REJECTION USING OPENED CIRCUIT STUBS AND Z-SLOTS DEFECTED GROUND STRUCTURES

Ashraf S. Mohra

Department of Electrical Engineering, College of Engineering, King Saud University, Saudi Arabia; Corresponding author: amohra@ksu.edu.sa

Received 23 June 2010

ABSTRACT: A new microstrip low pass filter (LPF) with defected ground structure (DGS) is proposed in this article. The DGSs consists of reshaped rectangular dumbbell slot and four groups of Z-shape slots. The microstrip line with DGS gave good rejection band extend from 3.0 to 9 GHz with acceptable pass band. The microstrip line with open circuit stubs (without DGS) gave good rejection band at the high frequency from 9 to 14 GHz. Using both structures results in LPF with wideband rejection from 3.37 to 14 GHz with attenuation less than (-26.0dB) and good passband less than (-25 dB). An equivalent circuit for the proposed LPF was given. The realized filter size was 34.0×34.0 mm², and it gave good agreement with simulated results. © 2011 Wiley Periodicals, Inc. *Microwave Opt Technol Lett* 53:811–815, 2011; View this article online at wileyonlinelibrary.com. DOI 10.1002/mop.25876

Key words: microstrip; defected ground structures; low pass filter; wideband rejection; Z-slot

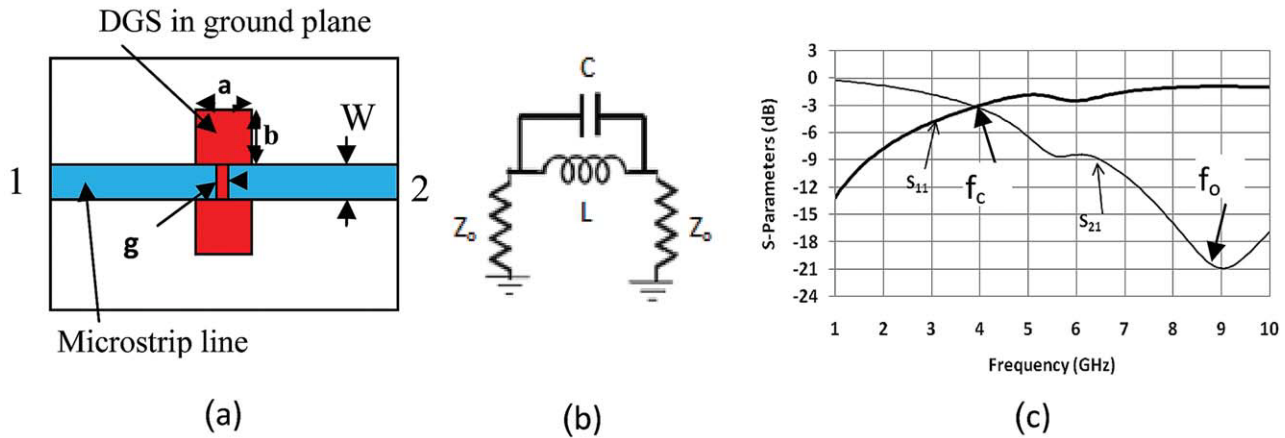


Figure 1 (a) DGS microstrip line; (b) Equivalent circuit; (c) Cutoff and attenuation frequencies. [Color figure can be viewed in the online issue, which is available at wileyonlinelibrary.com]

1. INTRODUCTION

A low pass filter (LPF) with wideband rejection is an important component in RF front-End subsystems for various wireless communication services to avoid interference with other wireless systems. The LPF can be implemented in different method such as using lumped parameters or by series connection of high-low stepped impedances microstrip line sections, and so forth. The high impedance sections suffer from the fabrication difficulties and the appearance of spurious band, low rejection levels and narrow rejection band. Since defected ground structure (DGS) was proposed by Park et al. [1, 2], it has been one of the most interest topics in the research of electromagnetism and microwave field. Recently, the filter designs are based on microstrip with DGS, or photonic bandgap (PBG), [3–5]. The PBG scheme [6] requires many parameters to design, and it is difficult to derive an equivalent circuit model, whereas DGS needs less parameters to design, and it is easy to obtain and evaluate its equivalent circuit model [6–9].

The DGS is realized by etching off a defected pattern from the ground plane, under the microstrip lines, so the electric and magnetic fields are redistributed, which result in redistribution of the electric and magnetic currents. According to that, the distributed inductance and capacitance are changed, so the effective permittivity of the substrate is changed also. Thus, an LC equivalent circuit can be used to model the proposed DGS loop circuit. The DGS cells have inherently resonant properties, so they have been used in filtering circuits to improve the stop and pass band characteristics. The transmission lines combined with DGS have a finite pass and rejection band like LPF, whereas the standard transmission lines have only the simple transmission characteristic over broadband.

In this article, a microstrip LPF with DGS was designed for wideband rejection by the using of reshaped rectangular dumbbell slot, Z-slots and opened circuit stubs. The open circuit stubs are needed to add shunt capacitances to the microstrip to avoid the degradation of the wideband rejection and modify the performance of the passband. The designed LPF has a sharp and wide rejection band extended from 3.37 to 14 GHz and at achieve a good acceptable passband.

2. SIMULATION OF LPF WITH DGS

The regular dumbbell DGS slot and its equivalent circuit, is shown in Figure 1 [9]. The equivalent circuit consists of parallel

inductance and capacitance, where L and C can be calculated as follows [10]:

$$C = \frac{5f_c}{\pi(f_o^2 - f_c^2)} \quad (1)$$

$$L = \frac{250}{C(\pi f_o)^2} \quad (2)$$

Where, C is measured in (pF), L in (nH), the frequencies f_o and f_c are the lowpass attenuation and cutoff frequencies measured in GHz, respectively. The DGS for the proposed LPF is shown in Figure 2. The defected ground slots consist of middle reshaped rectangular dumbbell slot and four Z-slots. The design was done on the RT/Duroid ($\epsilon_r = 2.2$, $H = 0.7874$ mm), where the 50Ω microstrip line width is 2.4 mm. In all the following cases, the width of microstrip line above the DGS increased to 4.4 mm to match the impedances. Here, the effect of each type of DGS will be studied separately as follows; the performance of the reshaped rectangular slot is shown in Figure 3. It achieves a cutoff frequency of 2.16 GHz and an attenuation frequency of 4.64 GHz, but the rejection band is limited up to 4.46 GHz when ($S_{21} < -15$ dB). The return and insertion loss for inner Z-slots added to the middle reshaped rectangular slot are shown in Figure 4. The cutoff frequency for this case is 2.98 GHz and the attenuation frequency is 3.84 GHz, while the rejection band is extended up to 8.5 GHz when ($S_{21} < -15$ dB).

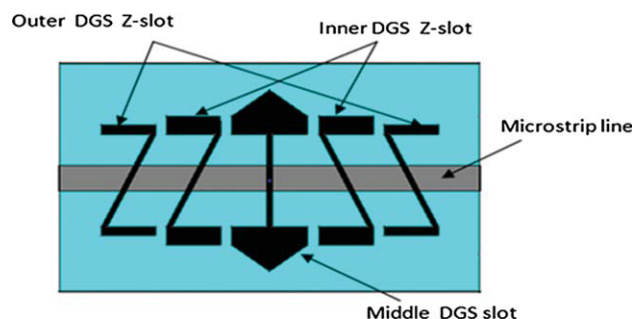


Figure 2 The Schematic of the microstrip line with DGS. [Color figure can be viewed in the online issue, which is available at wileyonlinelibrary.com]

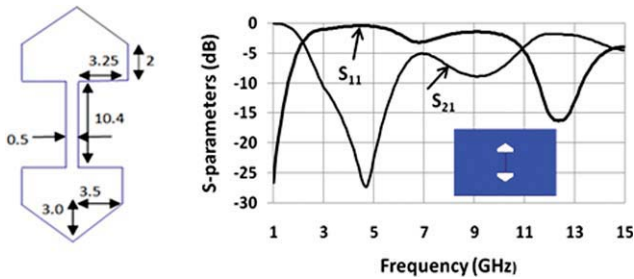


Figure 3 The Performance for reshaped rectangular DGS slot, all dimensions are in mm. [Color figure can be viewed in the online issue, which is available at wileyonlinelibrary.com]

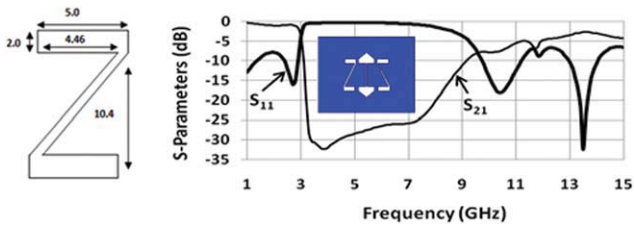


Figure 4 The performance of inner Z-slots with middle slot, all dimensions are in mm. [Color figure can be viewed in the online issue, which is available at wileyonlinelibrary.com]

When the outer Z-slots are simulated with the inner reshaped rectangular slot, Figure 5, it achieves 2.65 GHz cutoff frequency and 4.4 GHz attenuation frequency. The passband performance is better than case of inner Z-slots, and it achieves a good value ($S_{11} < -15$ dB) in all the band, but the rejection band deteriorates due to appearance of zero appear at 7.8 GHz.

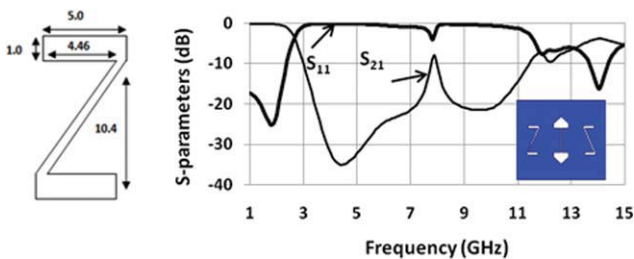


Figure 5 The performance of outer Z-slots with middle slot, all dimensions are in mm. [Color figure can be viewed in the online issue, which is available at wileyonlinelibrary.com]

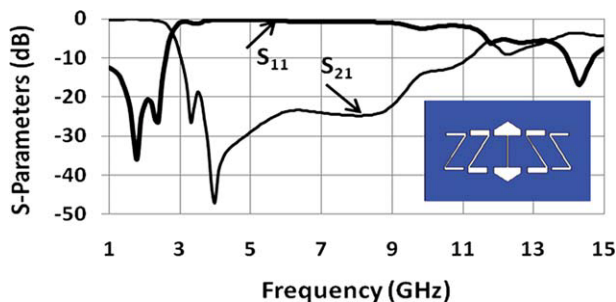


Figure 6 The S -parameters when using all of the DGS. [Color figure can be viewed in the online issue, which is available at wileyonlinelibrary.com]

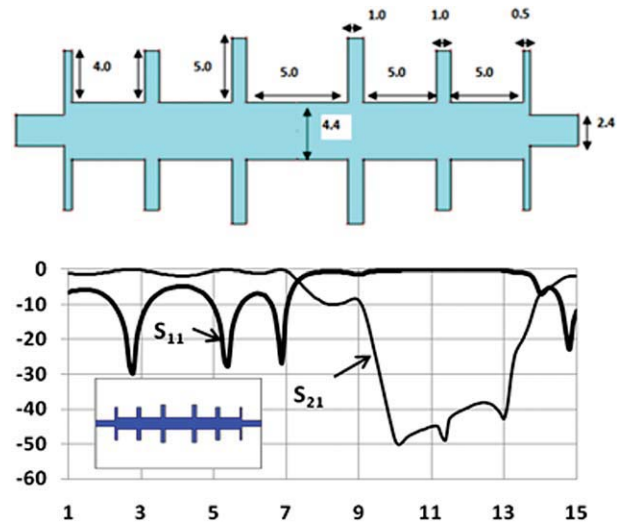


Figure 7 Microstrip line with open circuit stubs performance, all dimensions are in mm. [Color figure can be viewed in the online issue, which is available at wileyonlinelibrary.com]

The simulation of the filter when all defected ground slots are used is shown in Figure 6, where the separation between these slots is 1 mm. This configuration achieves 2.78 GHz cutoff frequency and 3.31 GHz attenuation frequency with rejection band up to 9.68 GHz and gave a deeper passband performance also.

To modify and extend the rejection band, some open circuit stubs are added to the microstrip line as shown in Figure 7. These open circuit stubs represent a parallel shunt capacitance that cause a good rejection band in the high frequency region that extend from 9.5 to 13.7 GHz. The simulated S -parameters for the proposed LPF that consists from all of the DGS slots and the microstrip line with open circuit stubs are shown in Figure 8. The proposed microstrip LPF achieve a wideband rejection from 3.37 to 14 GHz with attenuation ($S_{11} < -26.0$ dB) and a good passband ($S_{21} < -25.0$ dB).

3. EQUIVALENT CIRCUIT CALCULATIONS

Based on Eqs (1) and (2), the equivalent circuits for middle reshaped rectangular DGS is shown in Figure 9(a), where (f_c) was equal to 2.16 GHz, and (f_o) equal to 4.64 GHz. For inner single Z-slot, its equivalent circuit is shown in Figure 9(b),

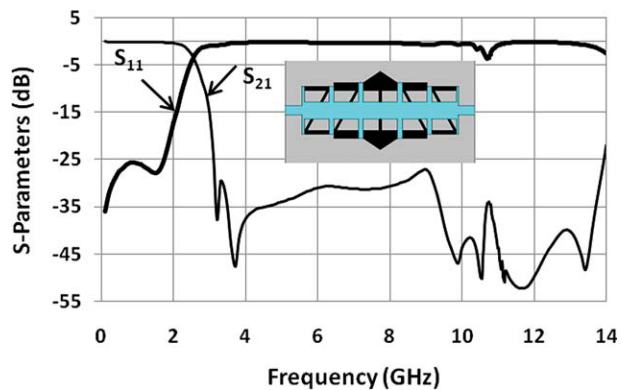


Figure 8 The S -parameters for microstrip line with open circuit stubs and all of DGS slots. [Color figure can be viewed in the online issue, which is available at wileyonlinelibrary.com]

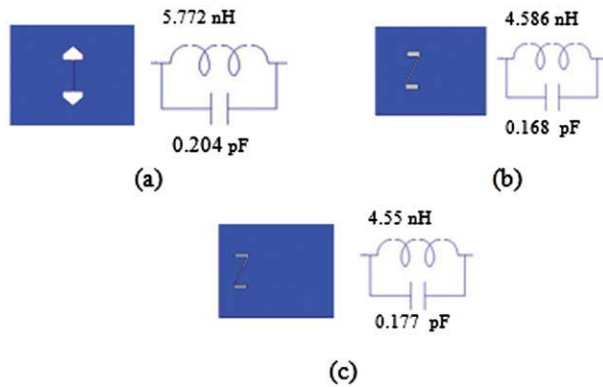


Figure 9 The equivalent circuit (a) Reshaped-Rectangular DGS slot; (b) Single inner Z-slot; (c) Single outer Z-slot. [Color figure can be viewed in the online issue, which is available at wileyonlinelibrary.com]

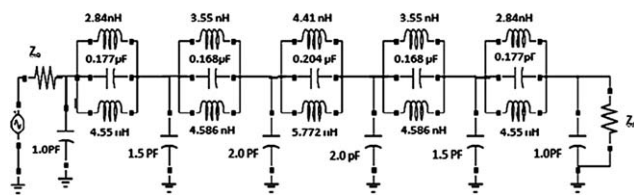


Figure 10 The equivalent circuit for the LPF with all of DGS slots

where (f_c) equal to 2.7 GHz, and (f_o) equal to 5.73 GHz. The equivalent circuit for single outer Z-slot is shown in Figure 9(c), with (f_c) equal to 2.69 GHz and (f_o) equal to 5.6 GHz. The open-circuit stubs that added on both sides of the microstrip line act as parallel capacitors. Due to the coupling between the different slots, an inductance was added to the parallel LC that represents each of DGS slots. The overall equivalent circuit parameters for the proposed LPF are calculated with IE3D software package [11], and it is shown in Figure 10. The S -parameters for the proposed LPF with DGS and the corresponding lumped element (LE) equivalent circuit are shown in Figure 11. The performance of both filter are in good agreement except that the LE have deviation at high frequency.

4. FABRICATION AND MEASUREMENTS

The proposed lowpass with DGS and open circuit stubs was realized on RT/Duroid 5880 ($\epsilon_r = 2.2$, $H = 0.7874$ mm). The photograph for the realized LPF is shown in Figure 12, while

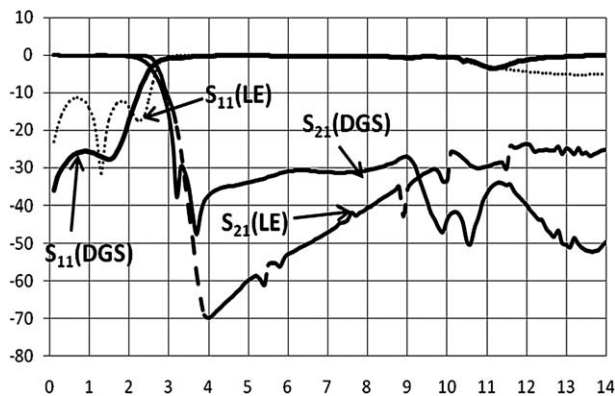


Figure 11 The S -Parameters for Filter with DGS and with lumped elements (LE)

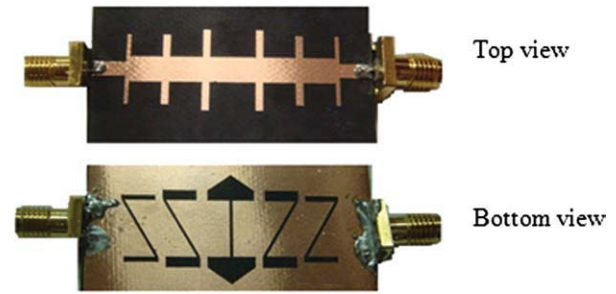


Figure 12 The photograph of the realized LPF with DGS slots. [Color figure can be viewed in the online issue, which is available at wileyonlinelibrary.com]

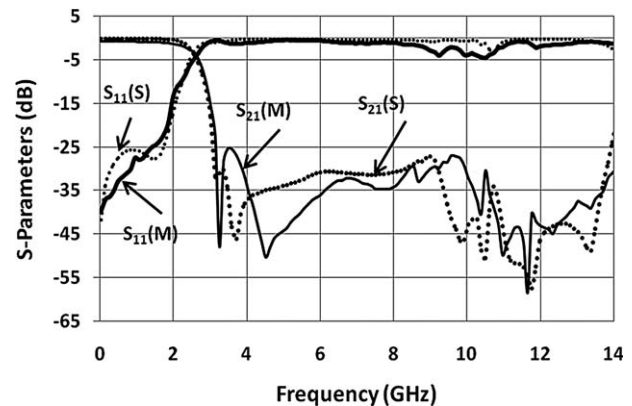


Figure 13 The measured and simulated S -parameters of the proposed LPF

the simulated (S) and the measured (M) scattering parameters are shown in Figure 13. The realized LPF performance is in good agreement with the simulated results. The realized LPF have a good passband, and it is less than (-25 dB) over the entire band. The cutoff frequency for the realized filter is around 2.62 GHz, so there is a shift in cutoff frequency with the simulated one by 30 MHz, which may be due to fabrication tolerance and mismatch due to measurement connectors. The realized filter have a wide rejection band from 3.37 GHz up to 14.0 GHz with value less than (-26.0 dB) over all band and achieve at the same time an acceptable passband.

5. CONCLUSION

The realized DGS LPF with DGS and open circuited stubs had a wider and deeper stopband characteristic than those of conventional LPF. The filter was consists of reshaped rectangular dumbbell slots added to four Z-slot with different sizes. The proposed LPF had a broad rejection band from 3.37 GHz up to 14 GHz with attenuation value less than (-26.0 dB) and good passband. An equivalent circuit for the proposed filter was given. The realized filter size is 34.0×34.0 mm², and it is in good agreement with simulated results.

ACKNOWLEDGMENTS

The author would like to acknowledge the assistance in fabrication and measurement provided by PSATRI (Prince Sultan for Advanced Technology Research Institute), King Saud University, Saudi Arabia.

REFERENCES

1. J.I. Park, C.S. Kim, J.S. Park, Y. Qian, D. Ahn, and T. Itoh, Modeling of a photonic bandgap and its application for the low pass filter design, *Asia Pacific Microwave Conf 2* (1999), 331–334.
2. D. Ahn, J. Park, C. Kim, Y. Qian, and T. Itoh, A design of the low pass filter using the novel microstrip defected ground structure, *IEEE Trans Microwave Theory Tech* 49 (2001), 86–93.
3. K. Saitoh, N. Florous, T. Muraio, S. Varshney, and M. Koshiba, Photonic bandgap filter design based on nonproximity resonant coupling mechanism, *IEEE Photonics Technol Lett* 19 (2007), 1547–1549.
4. Y. Xianbin, Z. Xiaoping, and Z. Hanyi, Microwave bandpass filter based on air core photonic bandgap filter loop mirror, *Microwave photonics*, MWP'06 (2006) 1–4.
5. J.S. Sun and G.Y. Chen, A High rejection lowpass filter servo photonic bandgap design, *Microwave Millimeter Wave Tech* (2004), 487–490.
6. J.-K. Lee, D.-H. Lee, and Y.-S. Kim, A compact lowpass filter with double step impedance shunt stub and defected ground structure for wideband rejection, *Microwave Opt Technol Lett* 52 (2010).
7. J.S. Lim, C.S. Kim, D. Ahn, Y.c. Jeong, and S. Nam, Design of lowpass filter using defected ground structure, *IEEE Trans Microwave Theory Tech* 53 (2005), 2539–2545.
8. A. boutejdar, A. Elsherbini, and A.S. Omar, Method for widening the reject band in lowpass/bandpass filters by employing coupled C-shaped defected ground structure, *IET Microwave Antenna propag* 2 (2008), 759–765.
9. A. Mohra, Compact lowpass filter with sharp transition using defected ground structure, *Prog Electromagnetic Res Lett* 8 (2009), 83–92.
10. Abdel-rahman, A. Boutjedar, A.K. Verma, G. Nadim, and A.S. Omar, Improved Circuit Model for DGS based lowpass Filter, *Antenna Propag Soc Int Symp* 1 (2004), 998–1001.
11. IE3D, Zeland Program manager, Ver. 9.35, Zeland software Inc., Fremont, CA U.S.A.

© 2011 Wiley Periodicals, Inc.

THEORETICAL INVESTIGATION OF TERAHERTZ AMPLIFIER BY CARBON NANOTUBES WITHIN TRANSMISSION LINE METAMATERIALS

Li-Ming Si, Hou-Jun Sun, and Xin Lu

Department of Electronic Engineering, School of Information Science and Technology, Beijing Institute of Technology, Beijing 100081, People's Republic of China; Corresponding author: siliming100@yahoo.com.cn

Received 25 June 2010

ABSTRACT: Terahertz (THz) power amplification in coplanar waveguide composite right left-handed transmission line (CPW CRLH TL) metamaterials with carbon nanotubes (CNTs) has been investigated. The negative differential resistance (NDR) behavior of the CNTs with appropriate DC voltage bias, which can be characterized as the feature of the Gunn-type oscillator, Esaki-like diode, or field effect transistor (FET), is used to provide the THz loss compensation/gain. From introducing gaps in the central signal line and short-circuited stubs connected between the CPW central signal line and the ground are used to realize the left-handed (LH) series capacitance C_L and LH shunt inductance L_L , respectively. The equivalent circuits model approach and effective medium method are employed to study the propagation constant $\gamma = \alpha + j\beta$ of the CNT-based active THz metamaterials, which are validated by three-dimensional (3D) full-wave finite element (FEM) and circuit model co-design. Results indicate not only the negative attenuation constant α (gain) provided by CNTs but also the negative

phase constant β (backward wave propagation with anti-parallel phase and group velocities) by artificial TL configuration at THz frequency region. This planar structure could be used to design tunable THz devices with different DC bias voltage and also easily extended to two-dimensional (2D) and 3D active microwave, IR, or optical metamaterials at room temperature. © 2011 Wiley Periodicals, Inc. *Microwave Opt Technol Lett* 53:815–818, 2011; View this article online at wileyonlinelibrary.com. DOI 10.1002/mop.25870

Key words: carbon nanotubes; composite right/left-handed transmission lines; active metamaterials; terahertz amplifier; negative refractive index; Bloch-Floquet theorem

1. INTRODUCTION

The terahertz (THz) spectrum typically includes the frequency range from 0.1 THz to 10 THz and is bound by the microwave and far-infrared (far-IR) regions. It is of great importance, as there are lots of advantages using this part of electromagnetic spectrum in the applications of many fields, such as THz imaging, spectroscopy, sensing, non-destructive detection, and short range radio communication [1]. However, many applications of THz are plagued by THz low-power generator and low-efficiency THz power amplifier, as well as strong absorption of THz in practical transmission medium, which have attracted much attention in recent years, especially the topic of how to amplify the THz power effectively. Several effective THz waves devices, such as THz sources using high temperature superconductor [2], THz zero-index quantum-cascade lasers [3], have been proposed, but they are obtained up to now only at very low temperature. Therefore, new technologies and novel materials are necessary to further ameliorate the THz devices and transmission systems with miniature size at room temperature.

Carbon nanotubes (CNTs) have attractive electronic properties as they can become either metallic or semiconducting, depending on the wrapping angle of graphene sheet (chiral angle) and diameter, described by the chiral index (n, m) , where n, m are integers [4]. When $n = m$, the CNT, termed armchair nanotube, is metallic, while $m = 0$, it, called zigzag nanotube, is generally semiconductor and is the only metal when n is an integer multiple of three (except these two types of CNTs, all are termed as chiral nanotubes). With (n, m) being specified, the diameter and the wrapping angle of graphene sheet of a CNT are known as $d = \frac{\sqrt{a}}{\pi} \sqrt{n^2 + m^2 + nm}$, $\theta = \sin^{-1} \left(\frac{\sqrt{3}m}{2\sqrt{n^2 + m^2 + nm}} \right)$, respectively, in which a is the Carbon–Carbon bond length, termed the lattice constant of graphene. The negative differential resistance (NDR) (electron transport characteristics) obtained from band gap/quantum tunneling effects and depended on the CNT diameter and lattice constant of graphene, of both metallic CNTs [5] and semiconducting CNTs [6] have been found and used for variety of molecular electronic devices and atomic-scale circuits, such as diodes, transistors, as well as high-speed electronic logic circuits at room temperature, which has commonly been considered that CNT is a possible successor to CMOS [7]. Moreover, for CNT junctions, although the current-voltage (I–V) curves of CNT chains are different in even and odd numbers of CNTs, the NDR is always existence for both even and odd chain junctions [8].

In the past decade, metamaterials exhibit many interesting properties not readily found in nature, such as negative/near-zero refraction [9, 10], optical magnetic permeability [11], and low-frequency electric permittivity [12], have attracted much attention from both fundamental and technological viewpoints. It has been achieved significant progress and extensively used in